Electronic Supplementary Material (ESI) for Inorganic Chemistry Frontiers.

Supporting Information

Ligand regulated metal−organic frameworks for synergistic photoredox and nickel catalysis

Yang Tang, Liang Zhao*, Guanfeng Ji, Yu Zhang, Cheng He, Yefei Wang, Jianwei Wei, and Chunying Duan

State Key Laboratory of Fine Chemicals, Zhang Dayu School of Chemistry, Dalian University of Technology, Dalian 116024, P. R. China

*Corresponding Author.
Email address: zhaol@dlut.edu.cn (L. Zhao)

Contents

1. Materials and Methods

2. Preparation of Metal─Organic Frameworks.

3. Single Crystal X-ray Crystallography.

4. Characterizations of Catalysts.

5. Catalysis Details.

6. References.

1. Materials and Methods

All the chemicals and solvents were of reagent grade quality obtained from commercial sources and used without further purification. Toluene used in this study was dried over sodium freshly distilled prior in the related reaction.

The elemental analysis of C, N, and H were performed on a Vario EL III elemental analyzer. FT-IR spectra were recorded from KBr pellets on ThermoFisher FT/IR-6700 instrument. The powder X-ray diffraction (PXRD) measurements were obtained on a Rigaku Smart Lab 9 kw X-ray diffractometer instrument with a Cu sealed tube in the angular range $2\theta = 5-50°$ at 293 K. Thermogravimetric analyses were performed on a Mettler-Toledo TGA/SDTA-851 instrument and recorded under N_2 followed by a ramp of 10 $°C\cdot min^{-1}$ up to 800 °C. NMR spectra were measured on Bruker Vaian DLG-400 spectrometers. ^1H NMR spectra were reported as follows: chemical shift (ppm, δ), multiplicity (s = singlet, d = doublet, t = triplet, q = quartet, m = multiplet, dd = double doublet, td = triple doublet), coupling constants (Hz), and numbers of protons. Solid UV-Vis spectra were recorded on Hitachi U-4100 UV-Vis-NIR spectrophotometer and a white standard of $BaSO_4$ was used as a reference. High-resolution mass spectra were collected on a Thermo Fisher Q Exactive Plus. Fluorescent spectra were recorded on Edinburgh FLS 920 stable/transient fluorescence spectrometer. All data about the photoluminescence decay were processed according to the following equation: $\tau = (A_1\tau_1^2 + A_2\tau_2^2) / (A_1\tau_1 + A_2\tau_2)$, τ_1 and τ_2 stood for the radiative lifetime and non-radiative lifetime respectively.[S1] Scanning electron microscopy (SEM) images were taken with a HITACHI UHR FE-SEM SU8200 Microscope and JSM-7610F Plus Field

Emission Scanning Electron Microscopy. Energy-dispersive X-ray spectroscopy (EDS) was taken with the JSM-7610F Plus Field Emission Scanning Electron Microscopy. The microstructure and morphology observations of samples were performed with Field Emission transmission electron microscope (TEM) of JEM-F200 operated at 200 kV. X-ray photoelectron spectroscopy (XPS) signals were collected on a Thermo ESCALAB Xi+ spectrometer. The absolute photoluminescence quantum yields (PLQY) were measured with an Edinburgh instruments FLS1000 fluorescence spectrometer by using an integrating sphere.

Solid-state cyclic voltammetry (CV) measurements were measured on ZAHNER ENNIUM Electrochemical Workstation by using a three-electrode system with an Ag/AgCl electrode as a reference electrode, a platinum silk with 0.5 mM diameter as a counter electrode, and a homemade carbon-paste electrode as a working electrode, in pH = 6.86 buffer solution at a scan rate of 100 $mV \cdot s^{-1}$. The manufacturing operation of carbon-paste working electrode: a well-ground mixture of sample and carbon paste (graphite and moderate mineral oil) was set in channel of a glass tube and connected to a copper wire. Cyclic Voltammetry of ligands were measured by using a graphite electrode as working electrode, Bu_4NPF_6 (0.1 M DMAc) was used as the supporting electrolyte.

Electrochemical impedance spectroscopy (EIS) measurements were measured on ZAHNER ENNIUM Electrochemical Workstation by using a three-electrode system with the sample-coated glassy carbon as the working electrode, platinum silk as counter electrode, and an Ag/AgCl as a reference electrode. The tetrabutylammonium hexafluorophosphate acetonitrile solution (0.05 M) was used as the electrolyte. The sample (4.0 mg) was dispersed into 15.0 μL 5 wt% Nafion, 0.5 mL ethanol, and 0.5 mL H_2O mixed solution, and the working electrode was prepared by dropping the suspension onto the surface of the glassy carbon electrode. The working electrode was dried, and then EIS measurements were performed with a bias potential of 0.8 V.

Photoelectrochemical measurements were performed on a CHI 660E electrochemical workstation using a standard three-electrode system with tetrabutylammonium hexafluorophosphate acetonitrile solution (0.05 M) as the electrolyte. The sample-coated glassy carbon as the working electrode, platinum silk as counter electrode, and an Ag/AgCl as a reference electrode. The sample (4.0 mg) was dispersed into 15.0 μL 5 wt% Nafion, 0.5 mL ethanol, and 0.5 mL H_2O mixed solution, and the working electrode was prepared by dropping the suspension onto the surface of the glassy carbon electrode. The photocurrent responses were measured at room temperature under the irradiation of a 420 nm LED (Ni−**PTA'**) and a 395 nm LED (Ni−**TCA'**), which were both purchased from the Beijing China Education Au-light Co., Ltd.

The charge density differences of Ni−**PTA** and Ni−**TCA** were obtained by using the Vienna Ab-initio Simulation Package (VASP) code.[S2−S5] For the total energy calculations, the plane wave cutoff energy was 400 eV. Ion-electron interactions were represented by ultrasoft pseudopotentials within the framework of the projector-augmented wave (PAW) method.[S6] The generalized gradient approximation (GGA) with the Perdew-Burke-Ernzerhof (PBE) functional was adopted as the exchange-correlation functional.[S6,S7] Ni−**PTA** and Ni−**TCA** were optimized until the energy was converged to 1×10^{-5} eV/atom and the forces smaller than 0.03 eV/Å. The Brillouin zone integration was approximated by a sum over special selected k-points using the 1×1×1 Monkhorst-Pack method.

2. Preparation of Metal−Organic Frameworks

Scheme S1. Synthesis procedure of ligand H_3**PTA**

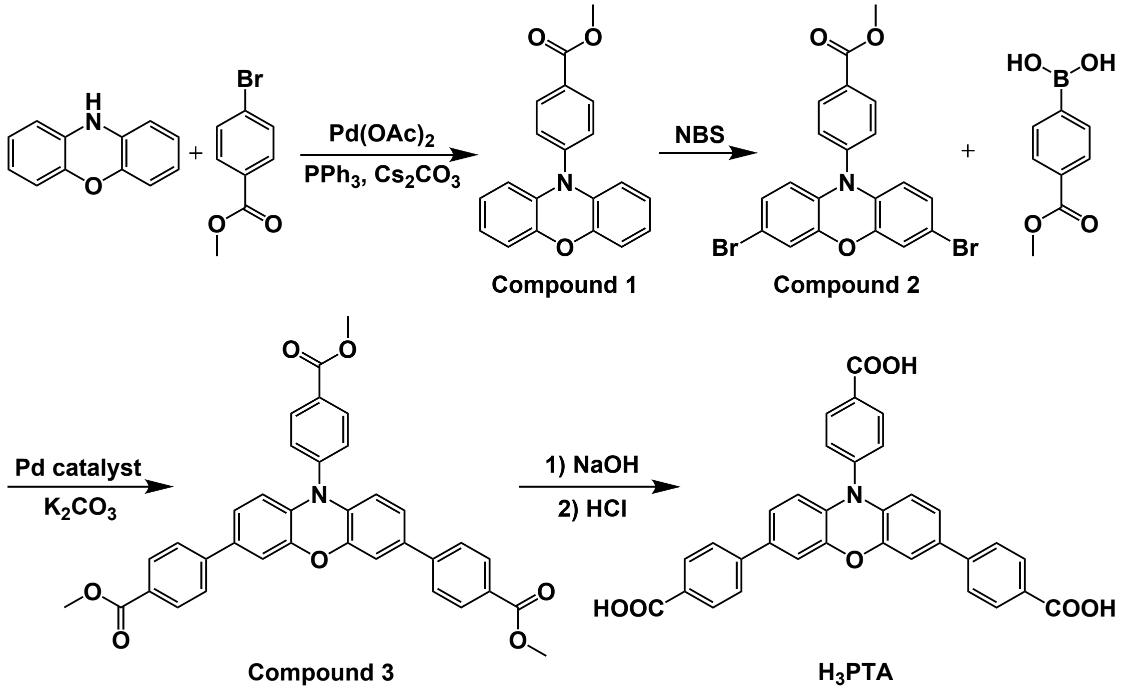

(1) Synthesis of methyl 4-(10*H*-phenoxazin-10-yl)benzoate (compound 1).

Methyl 4-bromobenzoate (2.11 g, 9.84 mmol), $Pd(OAc)_2$ (0.11 g, 0.49 mmol), Triphenylphosphine (PPh_3) (0.39 g, 1.49 mmol), Cs_2CO_3 (7.69 g, 23.60 mmol) and 10*H*-phenoxazine (1.50 g, 8.19 mmol) were dissolved in 100 mL of anhydrous toluene. The reaction mixture was refluxed with stirring for 24 hours under a nitrogen atmosphere, and then cooled to room temperature. The resulting mixture was poured into 200 mL water and extracted with dichloromethane (3 × 100 mL). The organic phase was washed with water (2 × 100 mL) and dried over anhydrous Na_2SO_4. After filtering, the filtrate was evaporated to dryness under reduced pressure. The crude was purified by chromatography on silica gel using ethyl acetate/petroleum ether (1:50, v:v) as the eluent to give compound 1. Yield: 80.3%. ^{1}H NMR (400 MHz, $CDCl_3$): δ 8.32−8.20 (m, 2H), 7.49−7.40 (m, 2H), 6.71 (dd, J = 7.8, 1.8 Hz, 2H), 6.67 (td, J = 7.5, 1.4 Hz, 2H), 6.59 (td, J = 7.7, 1.8 Hz, 2H), 5.92 (dd, J = 7.9, 1.4 Hz, 2H), 3.97 (s, 3H).

(2) Synthesis of methyl 4-(3,7-dibromo-10*H*-phenoxazin-10-yl)benzoate (compound 2).

Compound 1 (3.00 g, 9.46 mmol) was dissolved in chloroform (150 mL) and acetic acid (150 mL). *N*-bromosuccinimide (NBS) (3.46 g, 19.44 mmol) was slowly added to the mixture, which was left to stir at room temperature for 3 hours. The mixture was quenched with saturated Na_2CO_3 aqueous solution until pH = 7. After separation of phases, the organic layer was washed with water (3 × 100 mL) and brine (100 mL), dried over anhydrous Na_2SO_4. After filtering, the filtrate was evaporated to dryness under reduced pressure. The crude was purified by chromatography on silica gel using ethyl acetate/petroleum ether (1:4, v:v) as the eluent to give compound 2. Yield: 95.3%. ^{1}H NMR (400 MHz, $CDCl_3$): δ 8.27 (d, J = 7.3 Hz, 2H), 7.39 (d, J = 7.4 Hz, 2H), 6.82 (d, J = 16.2 Hz, 2H), 6.71 (d, J = 8.3 Hz, 2H), 5.76 (d, J = 8.2 Hz, 2H), 3.97 (s, 3H).

(3) Synthesis of trimethyl 4,4',4''-(10*H*-phenoxazine-3,7,10-triyl)tribenzoate (compound 3).

Compound 2 (2.15 g, 4.55 mmol), K_2CO_3 (2.50 g, 18.09 mmol), [1,1’-bis(diphenylphosphino)ferrocene]palladium(II) chloride (0.17 g, 0.23 mmol) and 4-(methoxycarbonyl)benzeneboronic acid (1.79 g, 9.94 mmol) were dissolved in a mixture containing 100 mL THF and 30 mL H_2O. The reaction mixture was refluxed with stirring for 24 hours under a nitrogen atmosphere, and then cooled to room temperature. The resulting mixture was poured into 100 mL of water and extracted with dichloromethane (3 × 100 mL). The organic phase was washed with water (2 × 100 mL) and dried over anhydrous Na_2SO_4. After filtering, the filtrate was evaporated to dryness under reduced pressure. The crude was purified by chromatography on silica gel using dichloromethane/petroleum ether (2:1, v:v) as the eluent to give compound 3. Yield: 67.5%. ^{1}H NMR (400 MHz, $CDCl_3$): δ 8.32 (d, J = 7.8 Hz, 2H), 8.05 (d, J = 7.7 Hz, 4H), 7.56 (d, J = 7.7 Hz, 4H), 7.50 (d, J = 7.7 Hz, 2H), 7.05 (s, 4H), 6.92 (d, J = 8.0 Hz, 4H), 6.03 (d, J = 8.0 Hz, 4H), 3.99 (s, 3H), 3.93 (s, 6H).

(4) Synthesis of 4,4',4''-(10*H*-phenoxazine-3,7,10-triyl)tribenzoic acid (H_3**PTA**).

Compound 3 (5.00 g, 8.54 mmol) and NaOH (5.13 g, 0.13 mol) were dissolved in a mixture containing 50 mL ethanol and 50 mL H_2O. The mixture was then refluxed for 24 hours. After cooling down to room temperature the mixture was acidified with HCl. The pH of the solution was adjusted to 3 to get the yellow precipitate. Finally, the precipitate was filtered and washed with plenty of water, dried in an oven to obtain the desired product. Yield: 92.7%. ^{1}H NMR (400 MHz, DMSO-d_6): δ 8.26 (d, J = 8.2 Hz, 2H), 7.96 (d, J = 8.2 Hz, 4H), 7.72 (d, J = 8.3 Hz, 4H), 7.64 (d, J = 8.2 Hz, 2H), 7.20 (d, J = 1.3 Hz, 2H), 7.13 (d, J = 8.4 Hz, 2H), 6.02 (d, J = 8.4 Hz, 2H). ^{13}C NMR (126 MHz, DMSO-d_6): δ 167.07, 166.59, 143.41, 142.78, 141.71, 133.00, 132.67, 132.40, 131.44, 130.59, 129.87, 129.14, 125.75, 122.40, 113.69, 113.68. Elemental analysis calcd for $C_{33}H_{21}NO_7$: C 72.92, H 3.89, N 2.58%. Found: C 72.99, H 4.15, N 2.64%.

(5) Preparation of Ni−**PTA**

A mixture of H_3**PTA** (27.20 mg, 0.05 mmol) and $NiCl_2\cdot6H_2O$ (13.07 mg, 0.055

mmol) were dissolved in water (1 mL) and *N*,*N*-dimethylacetamide (DMAc) (3 mL), which were placed in a 10 mL Teflon vessel within the autoclave. The mixture was heated at 85 °C for 72 hours and then cooled to room temperature at a rate of 2 $°C \cdot h^{-1}$. Green acicular crystals of Ni−**PTA** were obtained and collected from the mixture system above, washed with DMAc and air-dried. Yield: 60% (based on the crystal dried under room temperature). Elemental analysis calcd for $C_{41}H_{43}N_3O_{12}Ni$: C 59.39, H 5.19, N 5.07%. Found: C 59.62, H 5.09, N 4.68%. IR (KBr): 3408 (br, vs), 3050 (m), 1692 (m), 1603 (vs), 1524 (m), 1491 (s), 1401 (m), 1340 (m), 1290 (w), 1018 (m), 857 (m), 784 (s), 708 (m) cm^{-1}.

The crystal of Ni−**PTA** was dried under high vacuum at 70 °C for 5 hours to obtain the activated framework Ni−**PTA**' for catalytic experiments.

(6) Preparation of H_3**TCA**

The ligand 4,4′,4″-tricarboxytriphenylamine (H_3**TCA**) was synthesized using previously reported procedures and characterized by ^1H NMR. ^1H NMR data matched previously reported spectrum.[S8] ^1H NMR (400 MHz, DMSO-d_6): δ 7.91 (d, J = 8.3 Hz, 6H), 7.14 (d, J = 8.4 Hz, 6H).

(7) Preparation of Ni−**TCA**

A mixture of H_3**TCA** (18.85 mg, 0.05 mmol) and $Ni(NO_3)_2 \cdot 6H_2O$ (61.07 mg, 0.21 mmol) were dissolved in water (1 mL), methanol (1 mL) and *N*,*N*-dimethylformamide (4 mL), which were placed in a 10 mL Teflon vessel within the autoclave. The mixture was heated at 110 °C for 3 days and then cooled to room temperature at a rate of 3 $°C \cdot h^{-1}$. Green block crystals of Ni−**TCA** were obtained and collected from the mixture system above. Yield: 12% (based on the crystal dried under room temperature). Elemental analysis calcd for $C_{42}H_{36}N_2Ni_4O_{19}$: C 45.50, H 3.25, N 2.53%. Found: C 45.13, H 3.17, N 2.48%. IR (KBr): 3415 (br, s), 3193 (br, s), 1596 (vs), 1536 (m), 1506 (w), 1390 (vs), 1319 (m), 1269 (w), 1178 (vs), 1107 (w), 1013 (w), 884 (m), 784 (s), 676 (m), 527 (m) cm^{-1}.

The crystal of Ni−**TCA** was dried under high vacuum at 70 °C for 5 hours to obtain the activated framework Ni−**TCA'** for catalytic experiments.

3. Single Crystal X-ray Crystallography

The intensities of Ni−**PTA** and Ni−**TCA** were collected on a Bruker SMART APEX CCD diffractometer equipped with a graphite-monochromated Mo-Kα (λ = 0.71073 Å) radiation source; the data were acquired using the SMART and SAINT programs.[S9,S10] The structure was solved by direct methods and refined by full matrix least-squares methods by the program SHELXL-2014.[S11]

In the structural refinement of Ni−**PTA** and Ni−**TCA**, all the non-hydrogen atoms were refined anisotropically. Hydrogen atoms within the ligand backbones, DMAc and the coordinate water molecules were fixed geometrically at calculated distances and allowed to ride on the parent non-hydrogen atoms. The SQUEEZE subroutine in PLATON was used.[S12]

Table S1. Crystal data and structure refinements for all compounds.

Compound	Ni−**PTA**	Ni−**TCA**
Empirical formula	$C_{33}H_{19}NO_7Ni\cdot2C_4H_9NO\cdot3H_2O$	$C_{42}H_{26}N_2Ni_4O_{14}\cdot5H_2O$
M (g·mol^{-1})	828.49	1107.57
T (K)	200(2)	150(2)
Crystal system	Monoclinic	Orthorhombic
Space group	*P2(1)/c*	Aea2
a (Å)	18.944(10)	53.975(5)
b (Å)	26.245(14)	16.2783(16)
c (Å)	7.887(4)	18.3050(16)
α (°)	90	90
β (°)	101.763(12)	90
γ (°)	90	90
V (Å^3)	3839(4)	16083(3)
Z	4	8
D_{calcd} (g·cm^{-3})	1.433	0.915
μ (mm^{-1})	0.575	0.967
F (000)	1736	4528
Refl. collected/unique	36985 / 6753 [R_{int} = 0.0475]	120702 / 14126 [R_{int} = 0.0693]
Data / restraints / parameters	6753 / 0 / 518	14126 / 55 / 610
Goodness-of-fit on F^2	1.015	1.072
$R[I>2\sigma(I)]$[a]	R_1 = 0.0618 wR_2 = 0.1644	R_1 = 0.0352 wR_2 = 0.0906
R indices (all data)[b]	R_1 = 0.0795 wR_2 = 0.1743	R_1 = 0.0386 wR_2 = 0.0917
$\Delta\rho_{max,min}$ (eÅ^{-3})	0.573 / -0.605	0.757 / -0.495
CCDC Number	2130882	2130883

[a] $R_1 = \Sigma||F_o| - |F_c||/\Sigma|F_o|$; [b] $wR_2 = \Sigma[w(F_o^2 - F_c^2)^2]/\Sigma[w(F_o^2)^2]^{1/2}$

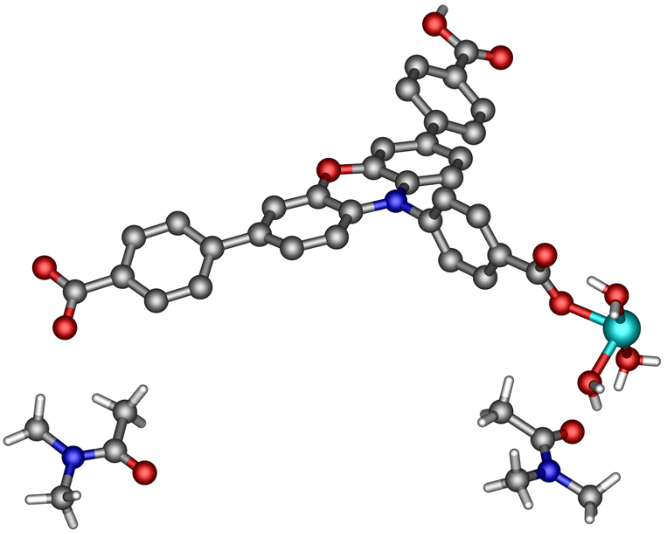

Figure S1. Single-crystal X-ray diffraction structure of Ni−**PTA** asymmetric unit. Ni cyan, C gray, O red, N blue, H white. Hydrogen atoms on the carbon atoms of ligand are omitted for clarity.

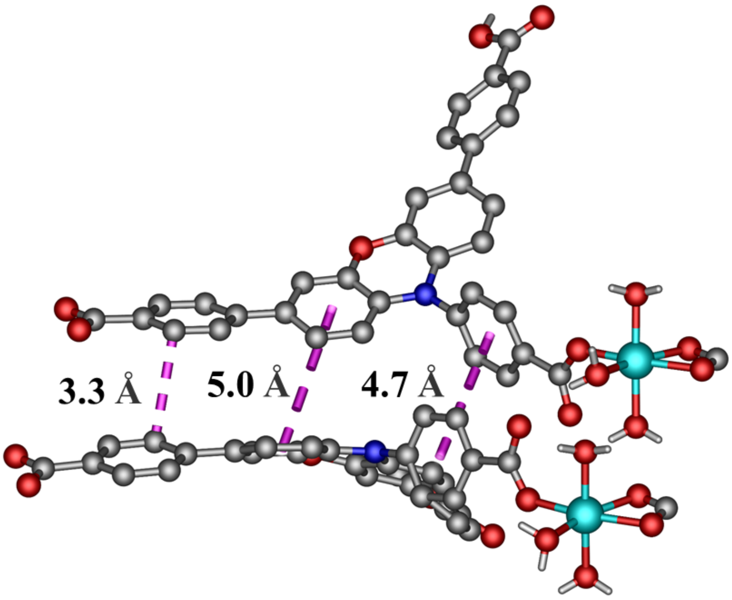

Figure S2. The multiple π···π interactions between the ligands in Ni−**PTA**. Ni cyan, C gray, O red, N blue, H white. DMAc molecules and hydrogen atoms on the carbon atoms of ligands are omitted for clarity.

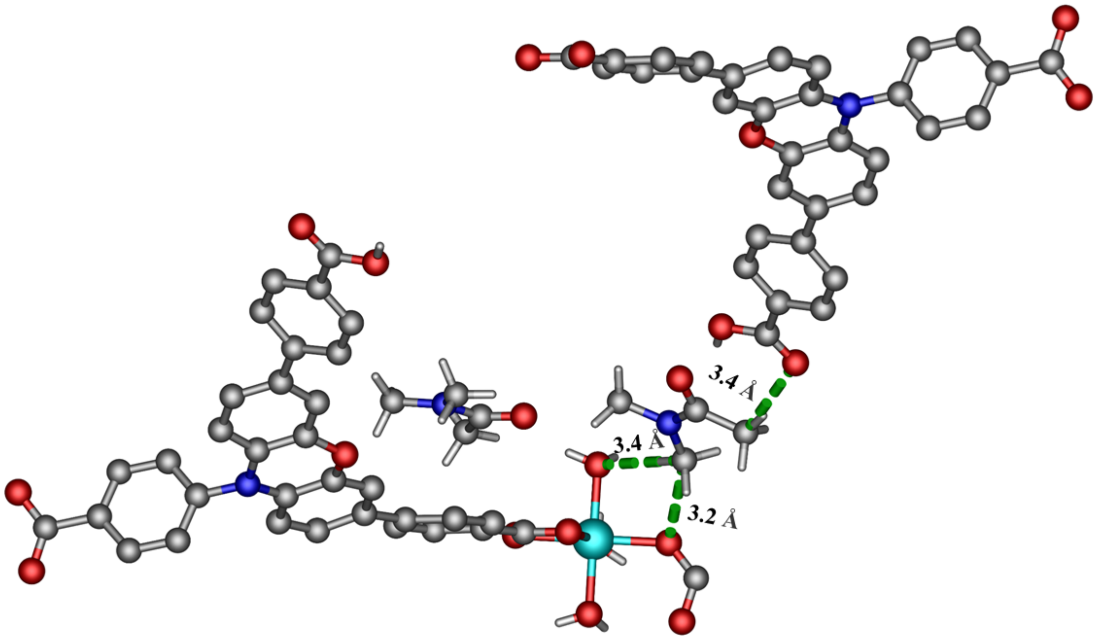

Figure S3. The multiple hydrogen bonds between DMAc molecules and ligands in Ni−**PTA**. Ni cyan, C gray, O red, N blue, H white. Hydrogen atoms on the carbon atoms of ligands are omitted for clarity.

Table S2. Selected bond lengths (Å) for Ni−**PTA**

Bond	Bond Length/Å	Bond	Bond Length/Å
Ni(1)-O(2W)	2.034(3)	Ni(1)-C(20)#1	2.449(4)
Ni(1)-O(1W)	2.036(3)	N(1)-C(21)	1.403(5)
Ni(1)-O(3W)	2.055(3)	O(1)-C(1)	1.268(4)
Ni(1)-O(1)	2.057(3)	O(7)-C(13)	1.382(4)
Ni(1)-O(4)#1	2.075(3)	C(1)-C(2)	1.510(5)
Ni(1)-O(3)#1	2.152(3)	C(2)-C(3)	1.387(5)

Table S3. Selected bond angles (°) for Ni−**PTA**

Bond	Bond Angle/°	Bond	Bond Angle/°
O(2W)-Ni(1)-O(1W)	89.85(12)	O(1W)-Ni(1)-O(3)#1	102.19(12)
O(2W)-Ni(1)-O(3W)	178.11(12)	O(2W)-Ni(1)-C(20)#1	90.91(12)
O(1W)-Ni(1)-O(3W)	92.03(11)	O(1W)-Ni(1)-C(20)#1	132.82(13)
O(2W)-Ni(1)-O(1)	89.27(10)	O(4)#1-Ni(1)-C(20)#1	31.70(12)
O(1W)-Ni(1)-O(1)	88.91(12)	C(21)-N(1)-C(8)	118.3(3)
O(3W)-Ni(1)-O(1)	90.53(10)	C(1)-O(1)-Ni(1)	129.8(2)
O(2W)-Ni(1)-O(4)#1	89.34(11)	C(20)-O(3)-Ni(1)#2	87.9(2)
O(1W)-Ni(1)-O(4)#1	164.46(11)	C(13)-O(7)-C(26)	116.8(3)
O(1)-Ni(1)-O(4)#1	106.60(12)	O(2)-C(1)-O(1)	124.8(3)
O(2W)-Ni(1)-O(3)#1	91.33(10)	O(2)-C(1)-C(2)	117.8(3)

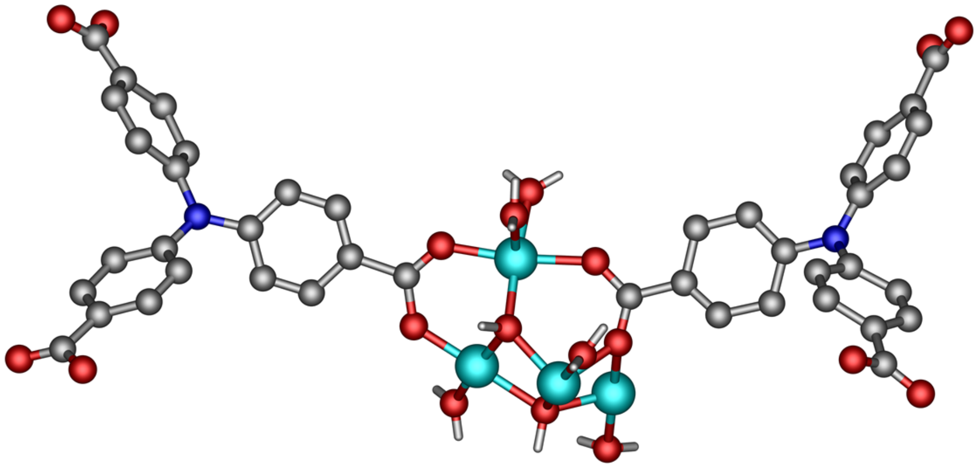

Figure S4. Single-crystal X-ray diffraction structure of Ni−**TCA** asymmetric unit. Ni cyan, C gray, O red, N blue, H white. Hydrogen atoms on the carbon atoms of ligands are omitted for clarity.

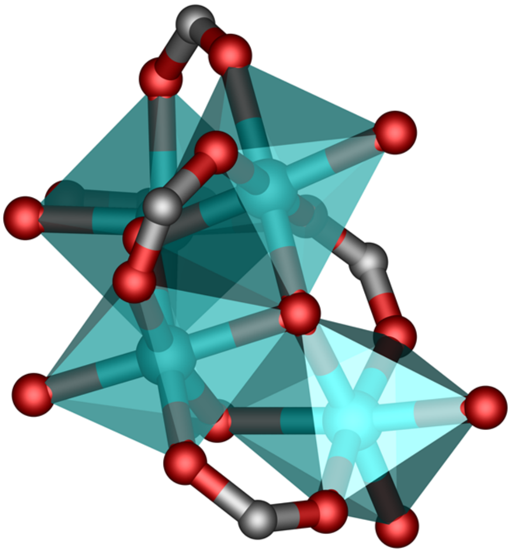

Figure S5. The coordinated environments and the polyhedral representation of tetranuclear [Ni_4].

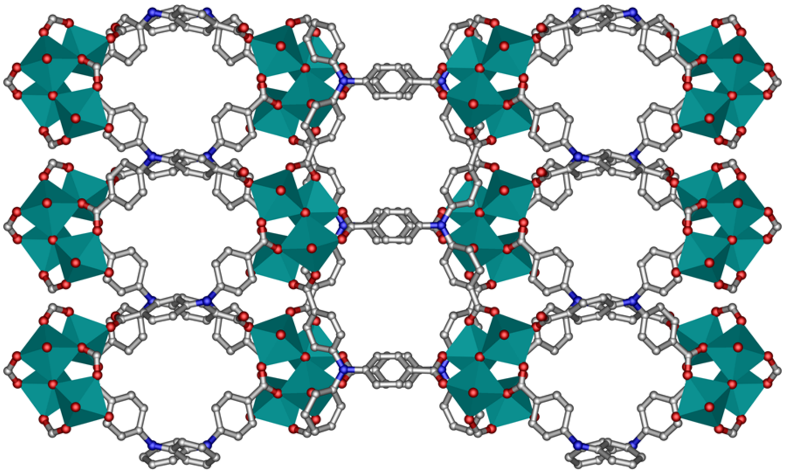

Figure S6. The view of the Ni−**TCA** along the b axis showing the mode of action of the stacking pattern of Ni−**TCA** fragments. Ni cyan, C gray, O red, N blue. Hydrogen atoms are omitted for clarity.

Table S4. Selected bond lengths (Å) for Ni−**TCA**

Bond	Bond Length/Å	Bond	Bond Length/Å
Ni(1)-Ni(4)#1	2.8849(7)	Ni(3)-O(8)#4	2.153(4)
Ni(1)-O(1)	1.933(3)	Ni(3)-O(9)	1.965(3)
Ni(1)-O(4)#1	2.020(3)	Ni(3)-O(12)#5	2.062(3)
Ni(1)-O(10)#2	2.090(3)	Ni(3)-O(1H)#4	1.993(3)
Ni(1)-O(1H)	2.098(3)	Ni(3)-O(4W)	2.092(4)
Ni(1)-O(2H)	2.032(3)	Ni(4)-O(3)	2.048(3)
Ni(1)-O(1W)	2.042(4)	Ni(4)-O(5)#1	2.100(3)
Ni(2)-O(2)	1.973(3)	Ni(4)-O(8)#6	2.109(3)
Ni(2)-O(7)	2.057(3)	Ni(4)-O(1H)#6	2.036(4)
Ni(2)-O(10)#2	2.121(3)	Ni(4)-O(2H)#6	1.967(3)
Ni(2)-O(2H)	2.040(3)	Ni(4)-O(5W)	2.086(4)
Ni(2)-O(2W)	2.124(4)	N(1)-C(5)	1.400(5)
Ni(2)-O(3W)	2.076(3)	O(1)-C(1)	1.340(6)
Ni(3)-O(6)#3	2.099(3)	C(1)-C(2)	1.542(6)

Table S5. Selected bond angles (°) for Ni−**TCA**

Bond	Bond Angle/°	Bond	Bond Angle/°
O(1)-Ni(1)-Ni(4)#1	135.43(9)	O(9)-Ni(3)-O(4W)	87.69(15)
O(1)-Ni(1)-O(4)#1	90.47(12)	O(12)#5-Ni(3)-O(6)#3	85.83(13)
O(1)-Ni(1)-O(10)#2	92.30(12)	O(12)#5-Ni(3)-O(8)#4	92.68(13)
O(1)-Ni(1)-O(1H)	179.39(14)	O(12)#5-Ni(3)-O(4W)	90.90(15)
O(1)-Ni(1)-O(2H)	94.89(12)	O(1H)#4-Ni(3)-O(6)#3	94.82(13)
O(1)-Ni(1)-O(1W)	89.59(13)	O(1H)#4-Ni(3)-O(8)#4	82.22(13)
O(4)#1-Ni(1)-Ni(4)#1	79.25(9)	O(1H)#4-Ni(3)-O(12)#5	174.84(15)
O(4)#1-Ni(1)-O(10)#2	171.55(13)	O(1H)#4-Ni(3)-O(4W)	94.24(15)
O(4)#1-Ni(1)-O(1H)	89.09(12)	O(4W)-Ni(3)-O(6)#3	86.93(15)
O(4)#1-Ni(1)-O(2H)	91.31(13)	O(4W)-Ni(3)-O(8)#4	174.13(13)
O(4)#1-Ni(1)-O(1W)	93.18(15)	O(3)-Ni(4)-Ni(1)#6	82.78(9)
O(10)#2-Ni(1)-Ni(4)#1	93.22(8)	O(3)-Ni(4)-O(5)#1	84.73(13)
O(10)#2-Ni(1)-O(1H)	88.20(12)	O(3)-Ni(4)-O(8)#6	172.70(14)
O(1H)-Ni(1)-Ni(4)#1	44.87(10)	O(3)-Ni(4)-O(5W)	92.25(14)
O(2H)-Ni(1)-Ni(4)#1	42.95(8)	O(5)#1-Ni(4)-Ni(1)#6	134.32(11)
O(2H)-Ni(1)-O(10)#2	80.50(12)	O(5)#1-Ni(4)-O(8)#6	89.30(13)
O(2H)-Ni(1)-O(1H)	85.54(12)	O(8)#6-Ni(4)-Ni(1)#6	98.51(10)
O(2H)-Ni(1)-O(1W)	173.63(14)	O(1H)#6-Ni(4)-Ni(1)#6	46.63(9)
O(1W)-Ni(1)-Ni(4)#1	133.80(10)	O(1H)#6-Ni(4)-O(3)	93.53(13)
O(1W)-Ni(1)-O(10)#2	94.82(14)	O(1H)#6-Ni(4)-O(5)#1	90.82(14)
O(1W)-Ni(1)-O(1H)	90.01(14)	O(1H)#6-Ni(4)-O(8)#6	82.33(14)
O(2)-Ni(2)-O(7)	172.51(14)	O(1H)#6-Ni(4)-O(5W)	172.72(14)
O(2)-Ni(2)-O(10)#2	93.78(14)	O(2H)#6-Ni(4)-Ni(1)#6	44.73(9)
O(2)-Ni(2)-O(2H)	94.36(13)	O(2H)#6-Ni(4)-O(3)	92.92(13)
O(2)-Ni(2)-O(2W)	87.34(15)	O(2H)#6-Ni(4)-O(5)#1	177.62(13)
O(2)-Ni(2)-O(3W)	89.16(14)	O(2H)#6-Ni(4)-O(8)#6	93.01(13)
O(7)-Ni(2)-O(10)#2	90.76(15)	O(2H)#6-Ni(4)-O(1H)#6	88.95(13)
O(7)-Ni(2)-O(2W)	88.76(16)	O(2H)#6-Ni(4)-O(5W)	95.16(13)
O(7)-Ni(2)-O(3W)	84.54(13)	O(5W)-Ni(4)-Ni(1)#6	138.81(9)
O(10)#2-Ni(2)-O(2W)	173.99(15)	O(5W)-Ni(4)-O(5)#1	85.32(14)
O(2H)-Ni(2)-O(7)	92.32(12)	O(5W)-Ni(4)-O(8)#6	91.45(15)
O(2H)-Ni(2)-O(10)#2	79.59(12)	C(1)-O(1)-Ni(1)	129.4(3)
O(2H)-Ni(2)-O(2W)	94.44(15)	C(8)-O(3)-Ni(4)	122.7(3)
O(2H)-Ni(2)-O(3W)	173.28(15)	C(8)-O(4)-Ni(1)#6	130.8(3)
O(3W)-Ni(2)-O(10)#2	94.48(15)	C(15)-O(5)-Ni(4)#6	133.1(3)
O(3W)-Ni(2)-O(2W)	91.44(17)	C(15)-O(6)- Ni(3)#7	125.8(3)
O(6)#3-Ni(3)-O(8)#4	88.70(15)	C(22)-O(7)-Ni(2)	136.4(3)
O(9)-Ni(3)-O(6)#3	169.25(13)	Ni(4)#1-O(8)-Ni(3)#2	91.30(13)
O(9)-Ni(3)-O(8)#4	97.25(15)	C(22)-O(8)-Ni(3)#2	124.4(4)
O(9)-Ni(3)-O(12)#5	84.96(13)	C(22)-O(8)-Ni(4)#1	133.0(3)
O(9)-Ni(3)-O(1H)#4	94.85(13)	C(29)-O(9)-Ni(3)	131.1(3)
Ni(1)#4-O(10)-Ni(2)#4	92.43(12)	C(29)-O(10)-Ni(1)#4	128.7(3)

C(29)-O(10)-Ni(2)#4	132.8(3)	C(5)-N(1)-C(19)	121.8(3)
C(36)-O(12)-Ni(3)#8	131.7(4)	C(12)-N(1)-C(19)	117.3(3)
O(2)-C(1)-C(2)	119.9(4)	O(1)-C(1)-C(2)	115.8(3)
C(4)-C(5)-N(1)	117.4(4)	O(2)-C(1)-O(1)	124.3(4)
C(4)-C(5)-C(6)	118.8(4)	C(26)-N(2)-C(33)	110.5(3)

4. Characterizations of Catalysts

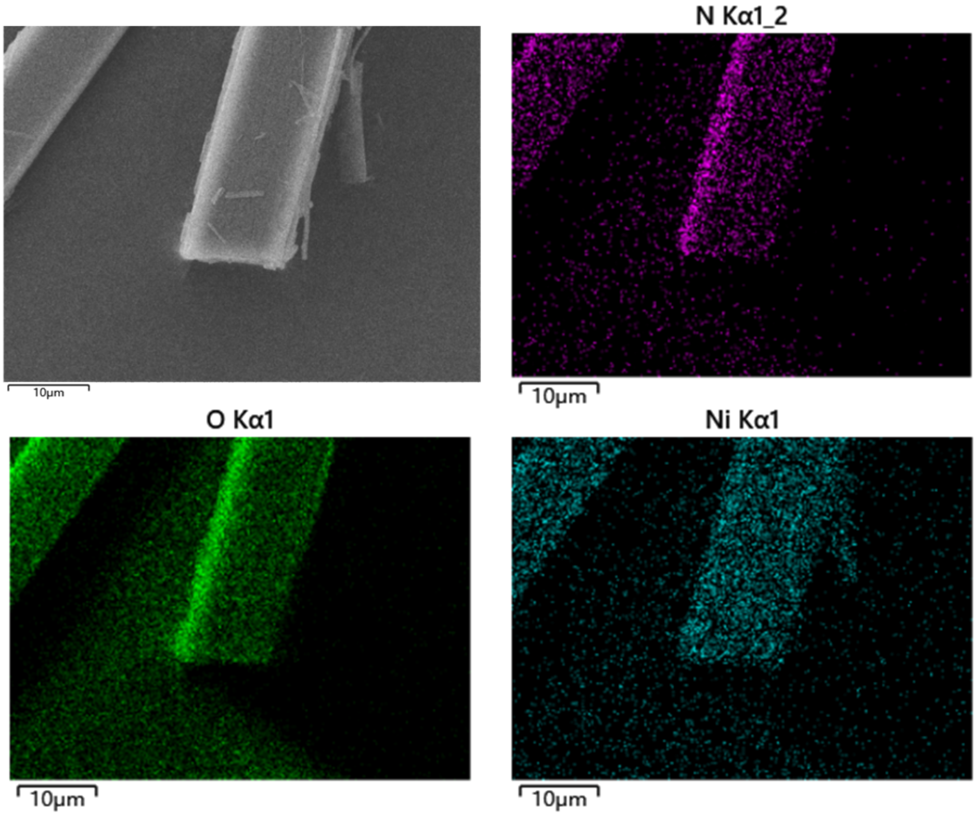

Figure S7. Element maps for Ni−**PTA'**.

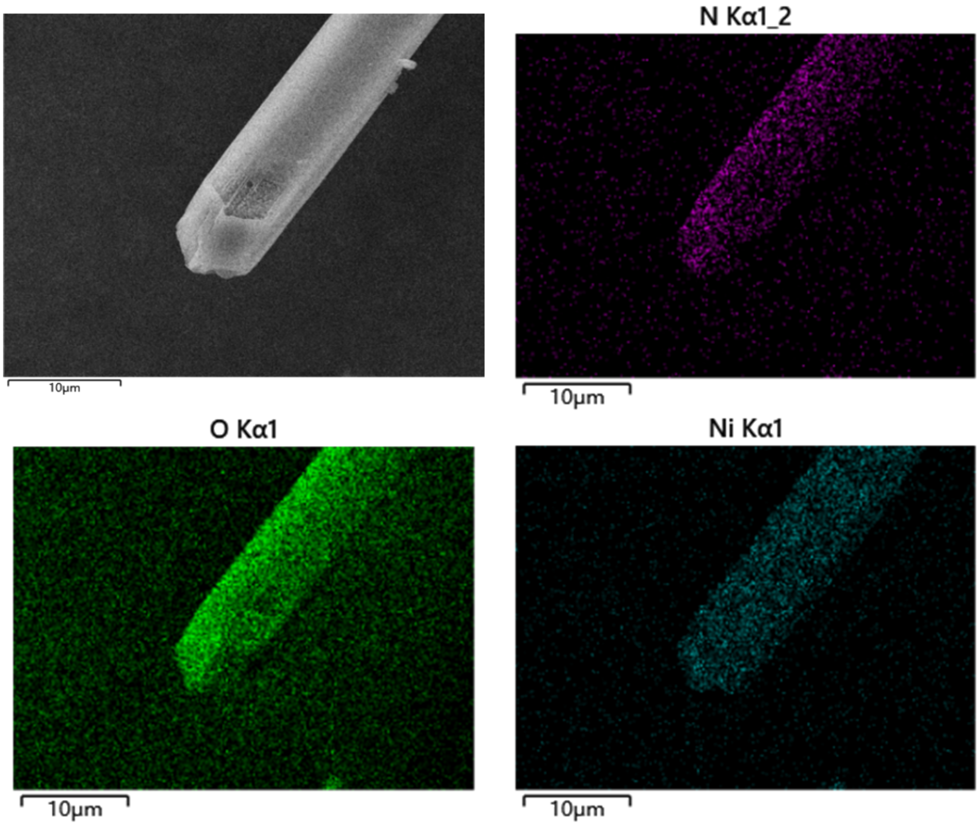

Figure S8. Element maps for Ni−**TCA'**.

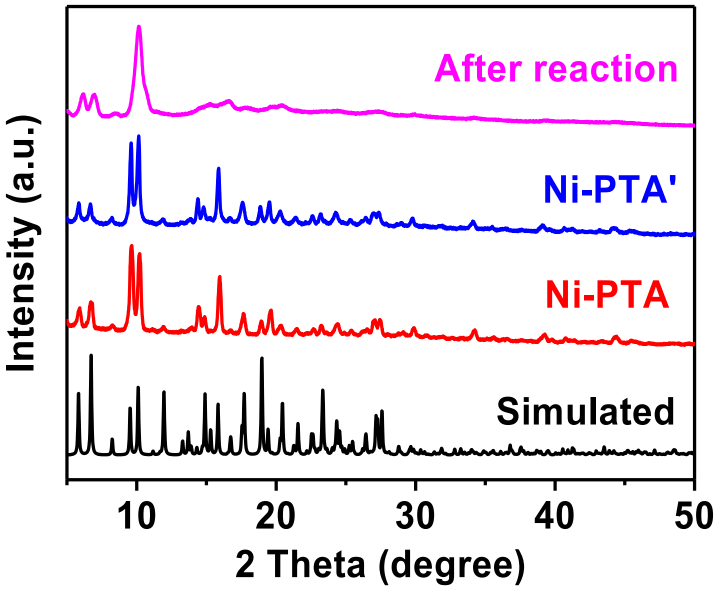

Figure S9. Powder XRD patterns of the single-crystal simulated Ni−**PTA** (black), the fresh as-synthesized Ni−**PTA** (red), the sample after activated (blue) and Ni−**PTA'** after reaction (pink).

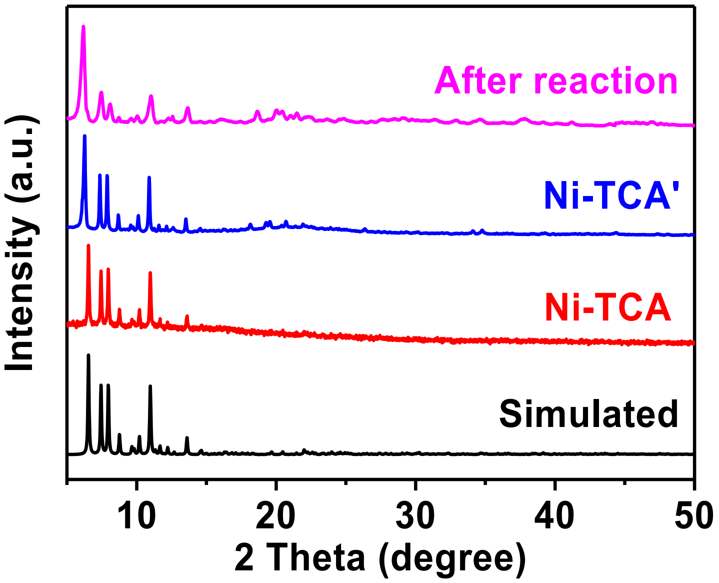

Figure S10. Powder XRD patterns of the single-crystal simulated Ni−**TCA** (black), the fresh as-synthesized Ni−**TCA** (red), the sample after activated (blue) and Ni−**TCA**' after reaction (pink).

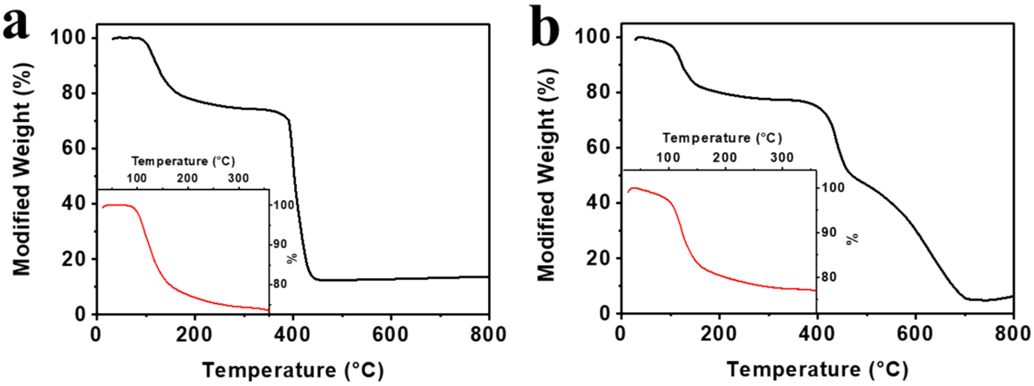

Figure S11. (a) Thermogravimetric analyses of Ni−**PTA** and (b) activated Ni−**PTA'**.

The samples were heated to 800 °C at a heating rate of 10 °C·min^{-1}.

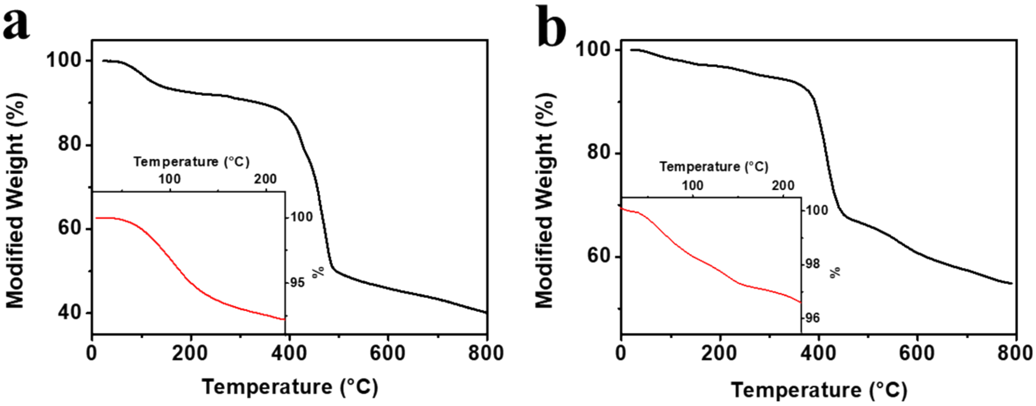

Figure S12. (a) Thermogravimetric analyses of Ni−**TCA** and (b) activated Ni−**TCA'**.

The samples were heated to 800 °C at a heating rate of 10 °C·min^{-1}.

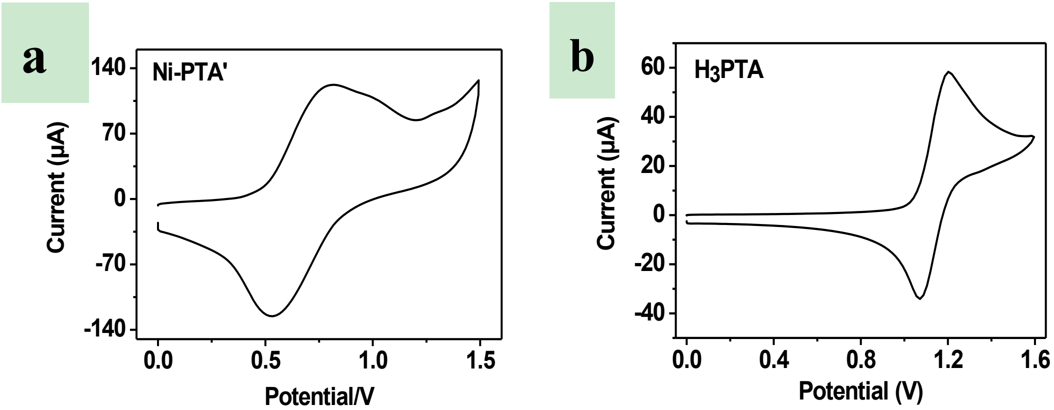

Figure S13. (a) Solid state cyclic voltammetry of Ni−**PTA'** in the range of 0~1.5 V with scan rates of 100 mV·s^{-1} in pH = 6.86 buffer solution and (b) of H$_3$**PTA** in the range of 0~1.6 V with scan rates of 100 mV·s^{-1} in DMAc.

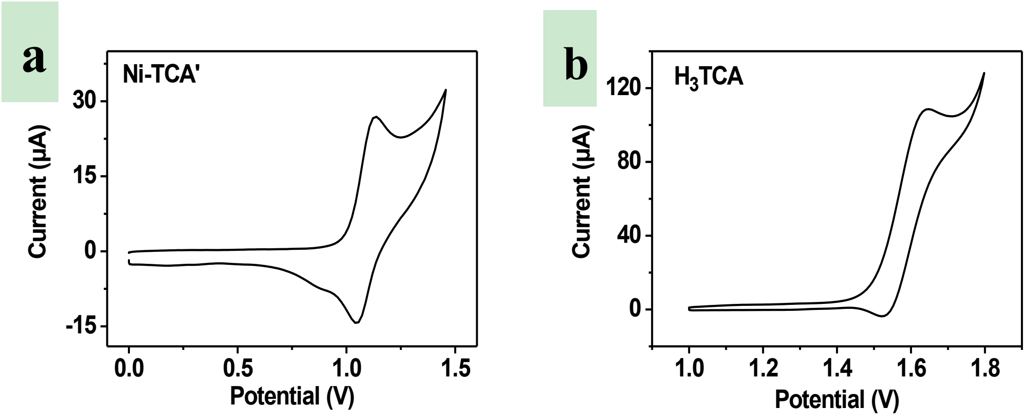

Figure S14. (a) Solid state cyclic voltammetry of Ni−**TCA'** in the range of 0~1.45 V with scan rates of 100 mV·s^{-1} in pH = 6.86 buffer solution and (b) of H_3**TCA** in the range of 0~1.8 V with scan rates of 100 mV·s^{-1} in DMAc.

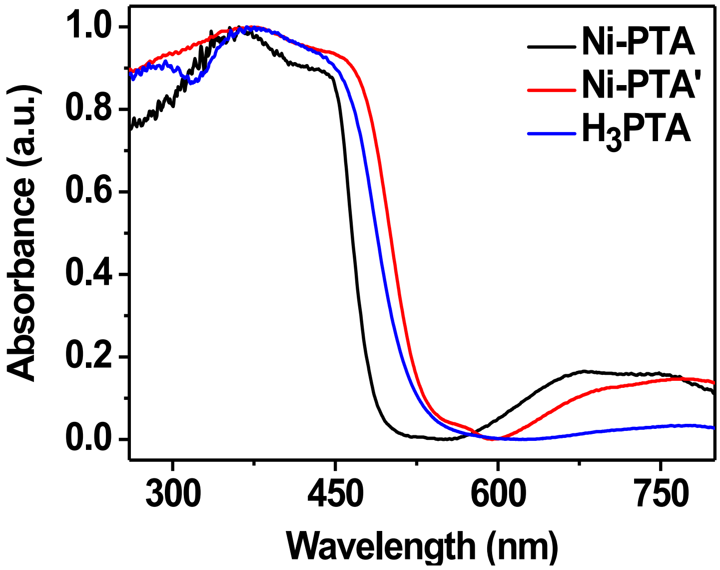

Figure S15. Solid UV-Vis spectra of H_3**PTA**, Ni−**PTA** and Ni−**PTA'**.

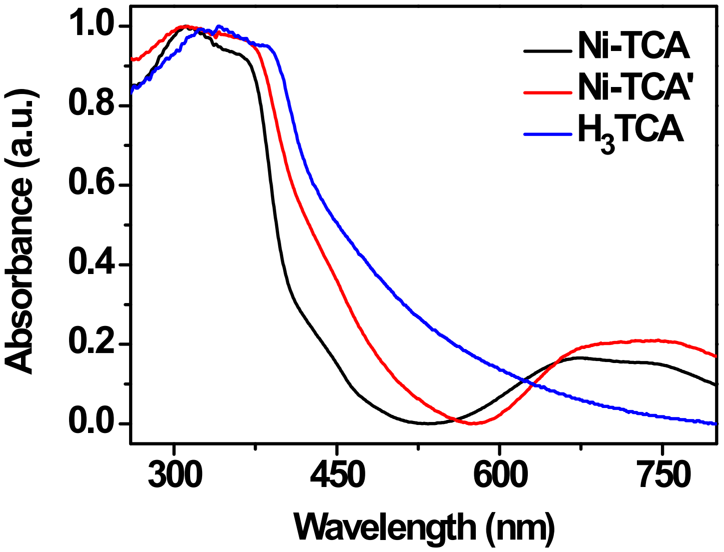

Figure S16. Solid UV-Vis spectra of H_3**TCA**, Ni−**TCA** and Ni−**TCA**'.

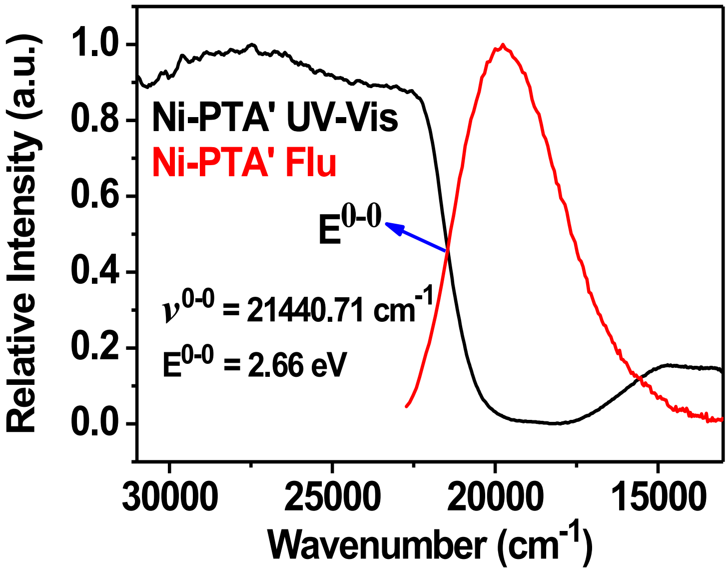

Figure S17. Solid state UV-Vis absorption and fluorescence emission spectra of Ni−**PTA**'. The fluorescence spectrum of Ni−**PTA**' in DMAc suspension was excited at 420 nm.

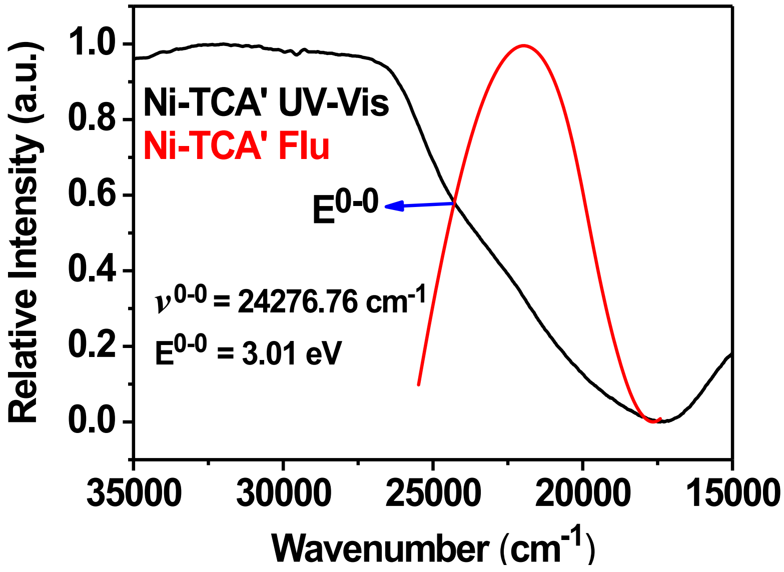

Figure S18. Solid state UV-Vis absorption and fluorescence emission spectra of Ni−**TCA'**. The fluorescence spectrum of Ni−**TCA'** in DMAc suspension was excited at 395 nm.

Table S6. Redox potentials and free energy changes of Ni−**PTA'** and Ni−**TCA'**

	$E_{1/2}$ (M^+/M)	E^{0-0}	E* (M^+/M^*)
Ni−**PTA'**	0.68 V	2.66 eV	−1.98 V
Ni−**TCA'**	1.09 V	3.01 eV	−1.92 V

$E^*_{1/2}(M^+/M^*) = E_{1/2}(M^+/M) - E^{0-0}$

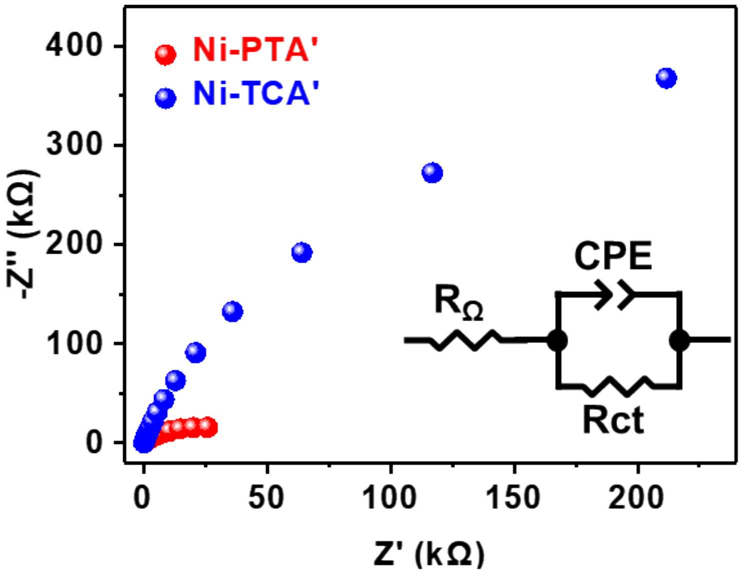

Figure S19. Electrochemical impedance spectroscopy plots of Ni−**PTA**' (red) and Ni−**TCA**' (blue) with a bias potential of 0.8 V.

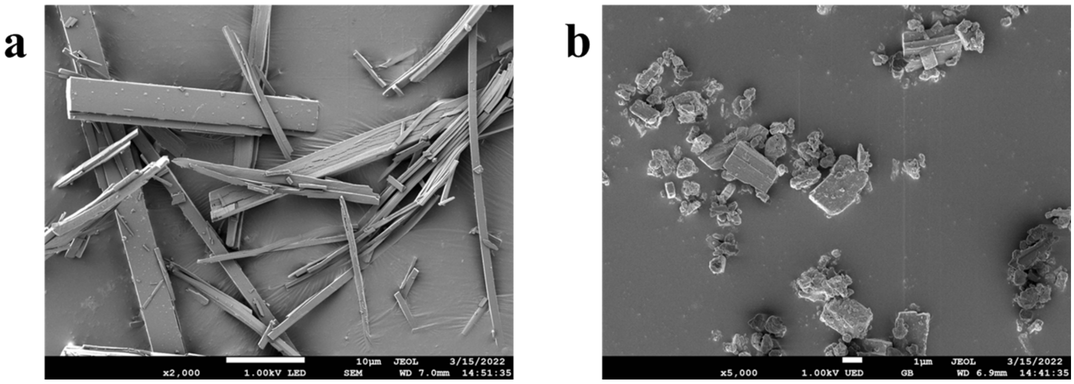

Figure S20. SEM photographs of Ni−**PTA'** before (a) and after (b) grinding showing the size change of catalyst.

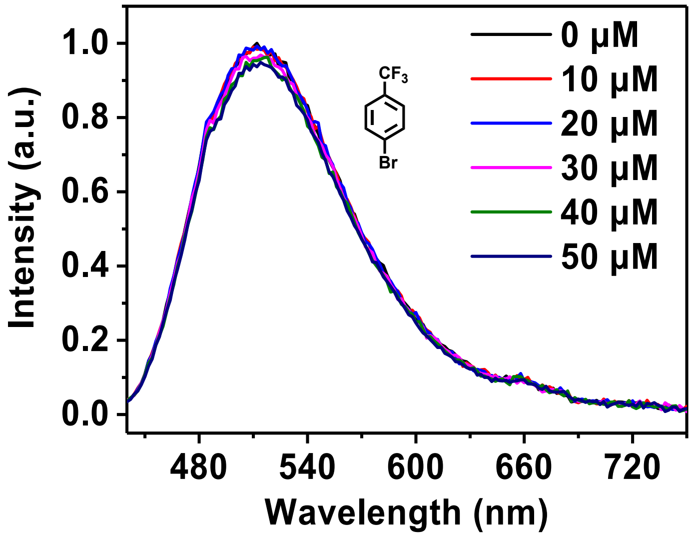

Figure S21. Fluorescence titration spectra of H_3**PTA** (10.0 μM) and $NiBr_2 \cdot 6H_2O$ (10.0 μM) in DMAc solution upon the addition of 1-bromo-4-(trifluoromethyl)benzene (50 μM), excitation at 420 nm.

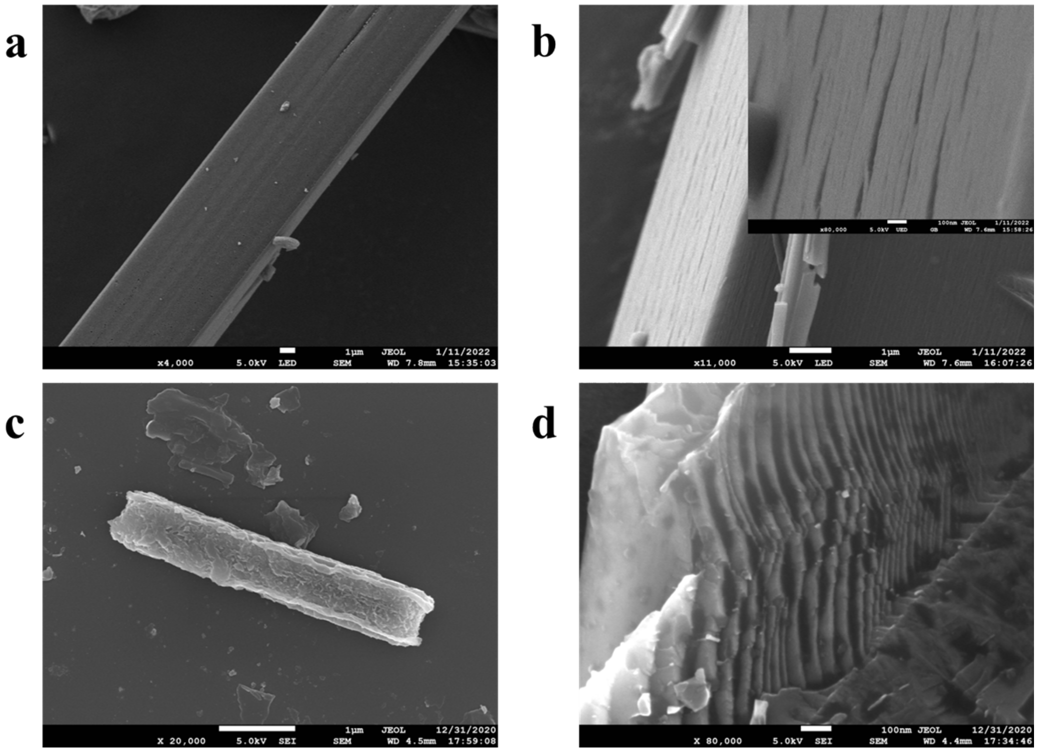

Figure S22. (a) SEM image of the initial Ni−**PTA'** crystals, displayed the Ni−**PTA'** crystals as prepared were the compact blocks. (b) Partial enlarged view of the initial Ni−**PTA'** crystals. (c) SEM image of the Ni−**PTA'** crystals after the photocatalytic reaction, displayed that Ni−**PTA'** was stripped from the bulk MOFs into thin sheets after photocatalysis. (d) Partial enlarged view of the Ni−**PTA'** crystals after the photocatalytic reaction.

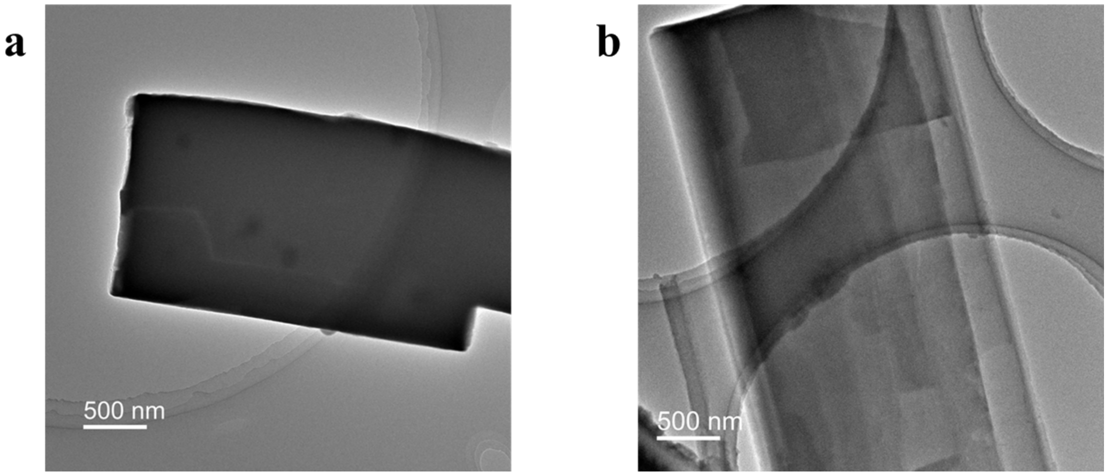

Figure S23. (a) TEM image of the initial Ni−**PTA'** crystals showed the crystals were thick blocks. (b) TEM image of the Ni−**PTA'** crystals after the photocatalytic reaction, showed the *in situ* exfoliation of Ni−**PTA'** to form thin layers.

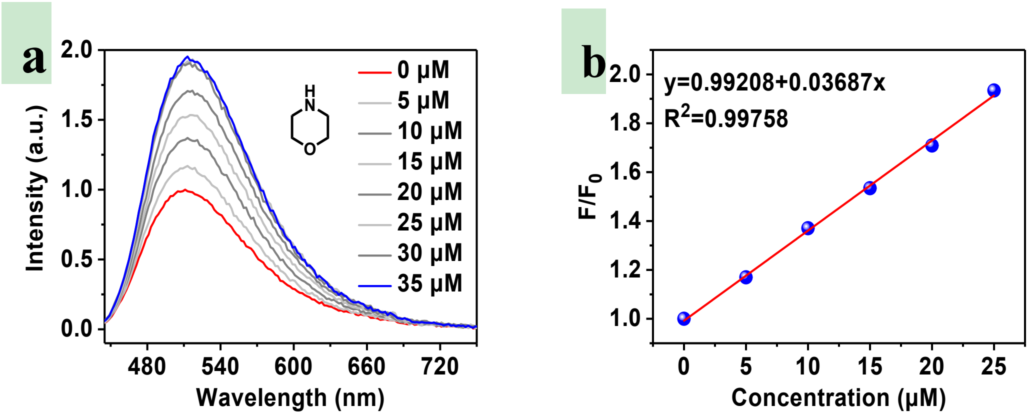

Figure S24. (a) Fluorescence titration spectra of Ni−**PTA'** in DMAc suspension upon the addition of morpholine (35 μM) and (b) the linear relationship between the fluorescence intensity and morpholine concentration. Fluorescence intensity were recorded at 512 nm, excited at 420 nm.

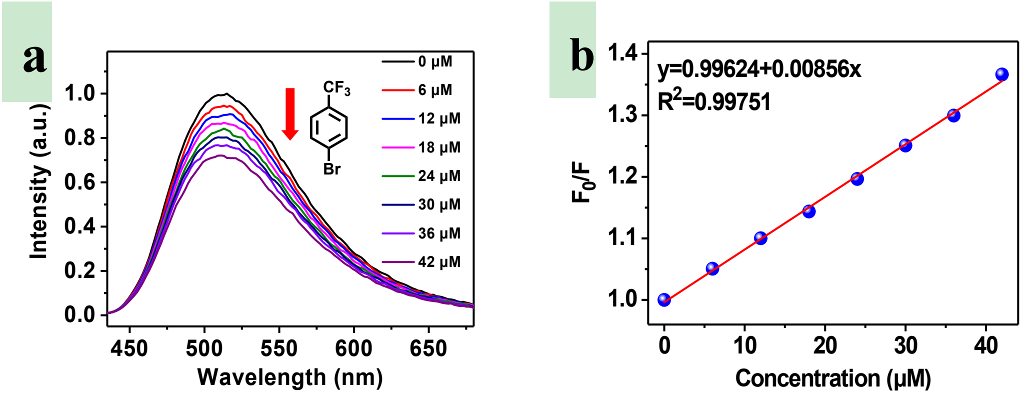

Figure S25. (a) Fluorescence quenching spectra of Ni−**PTA'** in DMAc suspension upon the addition of 1-bromo-4-(trifluoromethyl)benzene (42 μM) (b) The corresponding simulated Stern-Volmer curve. Fluorescence intensity were recorded at 512 nm, excited at 420 nm.

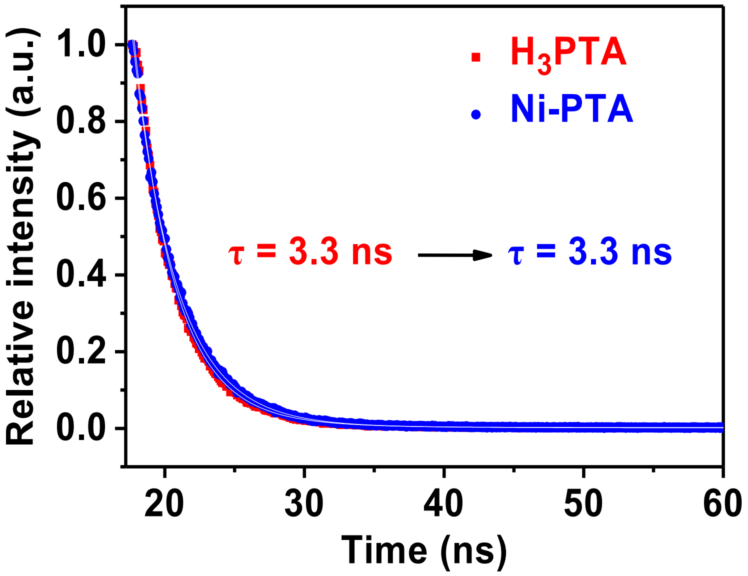

Figure S26. Time-dependence luminescence decay of H_3**PTA** solution (red) and Ni−**PTA'** suspension (blue). The intensity was recorded at 513 nm (H_3**PTA** solution) or 512 nm (Ni−**PTA'** suspension) with the excitation at 405 nm. The white line in the center of each line was the corresponding simulated one.

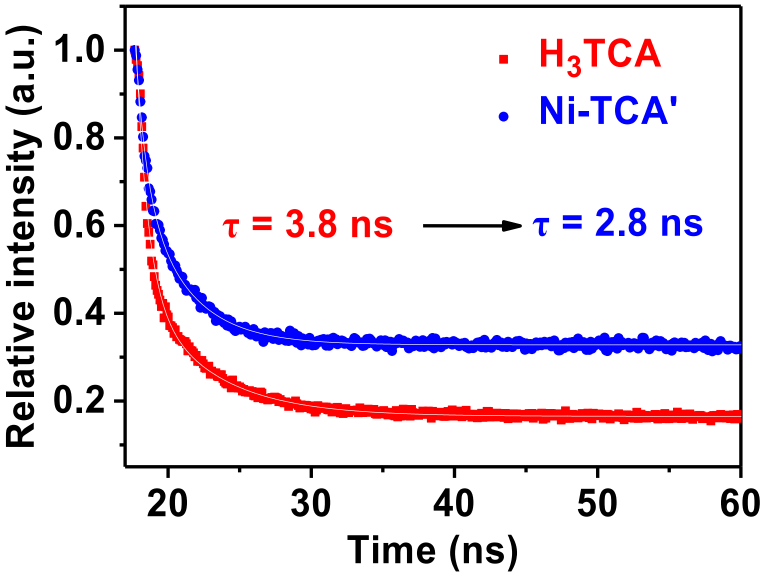

Figure S27. Time-dependence luminescence decay of H_3**TCA** solution (red) and Ni−**TCA'** suspension (blue). The intensity was recorded at 413 nm (H_3**TCA** solution) or 444 nm (Ni−**TCA'** suspension) with the excitation at 405 nm. The white line in the center of each line was the corresponding simulated one.

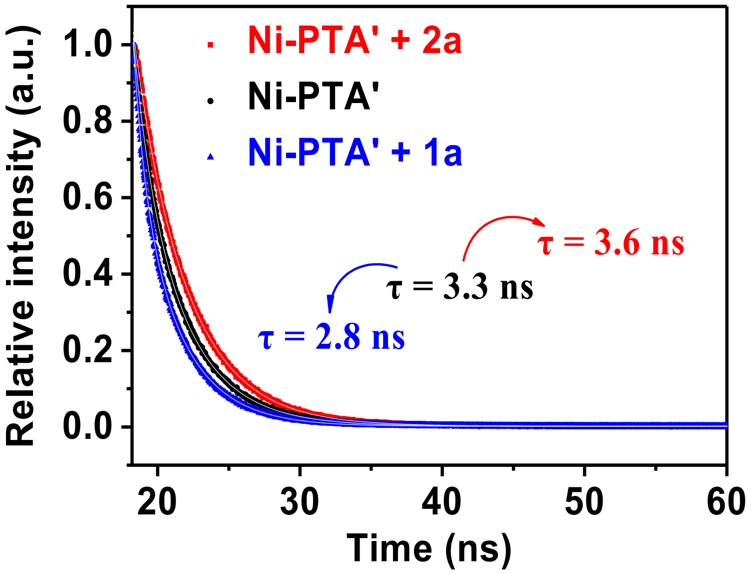

Figure S28. Time-dependence luminescence decay of Ni−**PTA'** suspension in DMAc and Ni−**PTA'** suspension with 4-bromobenzotrifluoride (**1a)**, the intensity was recorded at 512 nm with the excitation at 405 nm. And Ni−**PTA'** suspension with morpholine (**2a**) was recorded at 518 nm with the excitation at 405 nm. The white line in the center of each line was the corresponding simulated one.

Table S7. Fluorescence lifetimes of H_3**TCA**, Ni−**TCA'**, H_3**PTA**, Ni−**PTA'**, Ni−**PTA'** with **1a** and Ni−**PTA'** with **2a**.

Photocatalyst	A_1 (%)	τ_1 (ns)	A_2 (%)	τ_2 (ns)	τ (ns)
H_3**TCA**	66.7	0.83	33.3	4.83	3.8
Ni−**TCA'**	45.6	0.75	54.4	3.25	2.8
H_3**PTA**	93.3	2.79	6.7	6.38	3.3
Ni−**PTA'**	26.7	2.25	73.3	3.55	3.3
Ni−**PTA'** with **1a**	30.4	0.79	69.6	3.06	2.8
Ni−**PTA'** with **2a**	52.7	3.59	47.3	3.59	3.6

5. Catalysis Details

Typical procedure for C−N cross-coupling reactions.

A flame-dried Schlenk quartz flask was filled with the respective aryl halide (0.18 mmol), Ni−**PTA'** (9.0 μmol), amine (2.34 mmol), K_2CO_3 (0.54 mmol), a mini-stirrer and dry DMAc (3 mL) as solvent. The resulting mixture was degassed with Ar bubbling for 20 minutes and then sealed. The quartz flask containing the reaction mixture was then subjected to 420 nm LED irradiation for 12 hours with fan cooling to maintain the flask at room temperature. After reaction, we monitored the yield of the C−N coupled product by using ^{19}F NMR. We withdrew a ~10 μL aliquot from the reaction mixture and diluted the sample with ~600 μL of deuterated chloroform before subjecting the sample to ^{19}F NMR spectroscopy. It was assumed that during the course of the reaction, the number of CF_3 groups in the reaction mixture is conserved, allowing the yields of the C−N coupled products to be calculated.[S11]

TEMPO trapping experiments.

A flame-dried Schlenk quartz flask was filled with the respective 1-bromo-4-(trifluoromethyl)benzene (0.18 mmol), Ni−**PTA'** (0.18 mmol), morpholine (2.34 mmol), K_2CO_3 (0.54 mmol), TEMPO (1.8 mmol), a mini-stirrer and dry DMAc (3 mL) as solvent. The resulting mixture was degassed with Ar bubbling for 20 minutes and then sealed. The quartz flask containing the reaction mixture was then subjected to 420 nm LED irradiation for 12 hours with fan cooling to maintain the flask at room temperature. The reaction mixture was analyzed by HRMS, which showed the exact molecular ion indicating the formation of the proposed TEMPO adduct to the aryl radical intermediate.

^{19}F NMR (400 MHz, $CDCl_3$) or ^{1}H NMR (400 MHz, $CDCl_3$) spectroscopic data for the products of C–N cross-coupling.[S13,S14]

3a: 4-(4-(trifluoromethyl)phenyl)morpholine

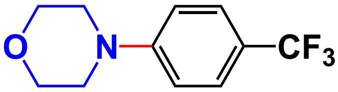

^{19}F NMR (376 MHz, $CDCl_3$): δ -61.4 (s, 3F). ^{19}F NMR data matched previously reported spectrum.[S13]

3b: *tert*-butyl 4-(4-(trifluoromethyl)phenyl)piperazine-1-carboxylate

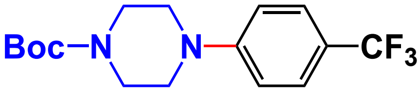

^{19}F NMR (376 MHz, $CDCl_3$): δ -61.4 (s, 3F). ^{19}F NMR data matched previously reported spectrum.[S13]

3c: 1-methyl-4-(4-(trifluoromethyl)phenyl)piperazine

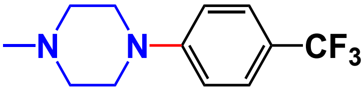

^{19}F NMR (376 MHz, $CDCl_3$): δ -61.4 (s, 3F). ^{19}F NMR data matched previously reported spectrum.[S14]

3d: 1-(4-(trifluoromethyl)phenyl)pyrrolidine

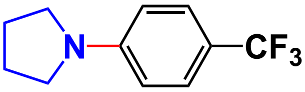

^{19}F NMR (376 MHz, $CDCl_3$): δ -60.6 (s, 3F). ^{19}F NMR data matched previously reported spectrum.[S13]

3e: 4-morpholinobenzonitrile

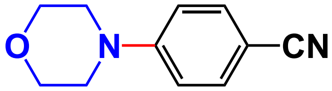

Typical procedure was followed using 4-bromobenzonitrile as the aryl halide, and morpholine as the amine. The reaction was run at room temperature for 12 hours. The filtrate was then evaporated to dryness under reduced pressure. Using 1,3,5-trimethoxybenzene as an internal standard (yield 70.8%). ^{1}H NMR data matched previously reported spectrum.[S13]

^{1}H NMR (400 MHz, CDCl$_3$): δ 7.54 − 7.45 (m, 2H), 6.89 − 6.81 (m, 2H), 3.83 (t, J = 5.2 Hz, 4H),3.27 (t, J = 5.2 Hz, 4H).

3f: *tert*-butyl 4-(3-(trifluoromethyl)phenyl)piperazine-1-carboxylate

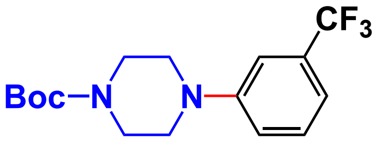

^{19}F NMR (376 MHz, CDCl$_3$): δ -62.8 (s, 3F). ^{19}F NMR data matched previously reported spectrum.[S13]

3g: 4-(3-(trifluoromethyl)phenyl)morpholine

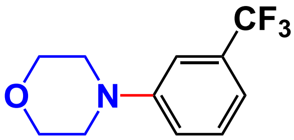

^{19}F NMR (376 MHz, CDCl$_3$): δ -62.8 (s, 3F). ^{19}F NMR data matched previously reported spectrum.[S13]

3h: *N*-(furan-2-ylmethyl)-4-(trifluoromethyl)aniline

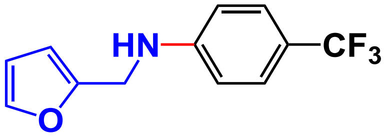

^{19}F NMR (376 MHz, CDCl$_3$): δ -62.8 (s, 3F). ^{19}F NMR data matched previously reported spectrum.[S13]

6. References

S1. W. J. Zhang, S. Z. Li, X. Tang, J. T. Tang, C. Y. Pan and G. P. Yu, Phenothiazine core promoted charge transfer in conjugated microporous polymers for photocatalytic Ugi-type reaction and aerobic selenation of indoles, *Applied Catalysis B: Environmental*, 2020, **272**, 118982–118991.

S2. G. Kresse and J. Furthmuller, Efficiency of ab-initio total energy calculations for metals and semiconductors using a plane-wave basis set, *Comput. Mater. Sci.*, 1996, **6**, 15−50.

S3. G. Kresse and J. Furthmuller, Efficient iterative schemes for ab-initio total-energy calculations using a plane-wave basis set, *Phys. Rev. B.*, 1996, **54**, 11169−11186.

S4. P. Hohenberg and W. Kohn, Inhomogeneous electron gas, *Phys. Rev.*, 1964, **136**, B864−B871.

S5. W. Kohn and L. J. Sham, Self-consistent equations including exchange and correlation effects, *Phys. Rev.*, 1965, **140**, 1133−1138.

S6. P. E. Blöchl, Projector augmented-wave method, *Phys. Rev. B: Condens. Matter.*, 1994, **50**, 17953−17979.

S7. J. P. Perdew, K. Burke and M. Ernzerhof, Generalized gradient approximation made simple, *Phys. Rev. Lett.*, 1996, **77**, 3865−3868.

S8. P. Y. Wu, C. He, J. Wang, X. J. Peng, X. Z. Li, Y. L. An and C. Y. Duan, Photoactive Chiral Metal−Organic Frameworks for Light-Driven Asymmetric α-Alkylation of Aldehydes, *J. Am.Chem. Soc.*, 2012, **134**, 14991−14999.

S9. SMART Data collection software (version 5.629); Bruker AXS Inc., Madison, WI, 2003.

S10. SAINT, Data reduction software (version 6.45); Bruker AXS Inc., Madison, WI, 2003.

S11. G. M. Sheldrick, SHELXTL97, Program for Crystal Structure Solution (University of Göttingen: Göttingen, Germany, 1997).

S12. A. L. Spek, Single-crystal structure validation with the program PLATON, *J. Appl. Cryst.*, 2003, **36**, 7−13.

S13. C. Lim, M. Kudisch, B. Liu and G. M. Miyake, C−N Cross-Coupling via Photoexcitation of Nickel-Amine Complexes, *J. Am. Chem. Soc.*, 2018, **140**, 7667−7673.

S14. F. Daili, S. Sengmany and E. Léonel, Amination of Aryl Halides Mediated by Electrogenerated Nickel from Sacrificial Anode, *Eur. J. Org. Chem.*, 2021, **17**, 2462−2469.